A simple and novel way of maintaining constant wall temperature in microdevices

V. S. Duryodhan[1], Abhimanyu Singh[1], Shiv Govind Singh[2], Amit Agrawal[1,*]

[1]Indian Institute of Technology Bombay, Powai, Mumbai, Maharashtra, India 400076

[2]Indian Institute of Technology Hyderabad, Hyderabad, Andhra Pradesh, India 502205

ABSTRACT

Constant wall temperature /homogeneity in wall temperature is the need of various lab-on-chip devices employed in biological and chemical investigations. In this work, a novel and simple way of maintaining constant wall temperature is proposed. A diverging microchannel along with conjugate effects are utilized towards this end. Both measurements and three dimensional numerical simulations are undertaken to prove the design. The investigation has been carried out over a large parameter range (divergence angle: 1-8°; length: 10-30 mm; depth: 86-200 μm; solid-to-fluid thickness ratio: 1.5-4.0, and solid-to-fluid thermal conductivity ratio: 27-646) and input conditions (mass flow rate: 2.5-5.5 ml/min, heat flux: 2.4-9.6 W/cm^2) which helped in establishing the finding. It is observed that a nearly constant wall temperature condition can be achieved over a large parameter range. A model is also proposed to arrive at the design parameter values. The method is demonstrated for Polymerase chain reaction (PCR) where we are able to maintain temperature each of the three stations within ±1 ºC. The finding is therefore significant and can be employed in both single and multi-stage processes requiring different constant wall temperatures with a fine resolution.

1. INTRODUCTION

The primary objective of this study is to propose a method for maintaining constant wall temperature in microdevices. In several biological applications, it is required to maintain the cells above/ below the room temperature implying the need for heating/ cooling the microdevice.

[*] Corresponding author: Dr. Amit Agrawal <amit.agrawal@iitb.ac.in>; Phone: +91 22 2576 7516

For instance, Hung et al. [1] designed a microfluidic cell culture array for studying the human carcinoma cells in which a constant temperature of 37 ^{o}C was required to be maintained. Wan et al. [2] studied proliferation and migration of tumor cells under a controlled temperature of 37 ^{o}C. Polymerase chain reaction (PCR) is a widely employed technique to amplify a particular DNA sequence and is used in a number of applications like pathogen detection [3,4] and hereditary disorder diagnosis [5]. The entire process takes place in three steps: denaturation, annealing and extension for which the different stations are required to be maintained at constant temperatures of 95, 55 and 72 ^{o}C, respectively. Selva et al. [6,7] required a certain temperature gradient in order to control the movement of bubbles and droplets by means of thermocapillary effects. These examples underline the need for developing an effective and efficient system which could maintain the microchannel walls at a desired temperature.

When the temperature of the sample is to be raised, as in the above examples, one can either supply a uniform heat flux at the boundaries, or maintain the boundaries at a higher temperature. As is well known, for hydrodynamically and thermally fully-developed flow in simple geometries, a uniform heat flux leads to a linear increase in surface temperature, and a constant difference between the bulk fluid and wall temperatures. The presence of a lateral temperature gradient in the fluid however implies that the local fluid temperature can exceed the safe operating temperature limit. Maintaining the boundaries at a constant temperature is therefore the safer alternative where the local fluid temperature will necessarily be less than the wall temperature (in the wall heated case). At the conventional scale, the constant wall temperature condition is typically maintained by employing phase change. Maintaining constant temperature is however not simple, more so when extended to microscale. Moreover, only certain temperatures (and not any desired temperature) can be achieved with the phase change technique due to the limitations in the material that can be employed for this purpose.

Hung et al. [1] and Wan et al. [2] employed an incubator to maintain constant surface temperature. The primary limitation of the approaches in [1-5] is that the device employed is bulky and cannot be readily integrated with a microdevice. Few research groups have tried to control the temperature gradients at microscale by using active control strategies. For example, Hsieh et al. [8] and Wang et al. [9] employed an array type of microheater with an active compensation unit. This is in contrast with the conventional block heater employed to achieve

constant wall temperature for PCR application. Persat and Santiago [10] employed an unconventional way of chemical cycling (reducing the melting temperature of DNA with addition of solvent) which reduces thermal cycling. Wu et al. [11] fabricated a microheater and a thermal sensor inside a PDMS microchannel using injection molding and demonstrated uniformity in temperature distribution with the help of high precision control system. Although they succeeded in their objective, the level of complexity associated in their approaches cannot be ignored. This defeats the primary reason of employing a microdevice in the first place. In this paper, we propose a much simpler solution to this problem.

2. PROPOSED DESIGN

An effect that becomes particularly relevant at the microscale is conduction in the walls (or conjugate effect), which leads to a redistribution of heat flux and temperature in both the flowing fluid and the solid walls [12-15]. In most of the conventional flow situations, the cross section through which fluid flows is much larger as compared to the wall thickness. The primary mode of heat transfer is convection and the magnitude of axial conduction within the solid is small as compared to convection through the fluid. However at the microscales, the characteristic dimensions of the microchannel are of the same order or may be smaller than the thickness of the substrate. When such a situation arises, the axial conduction through the solid cannot be neglected; heat transfer then happens by convection in the fluid coupled with axial conduction in the solid.

In several applications the bottom wall of the substrate is subjected to a constant heat flux boundary condition. If the conjugate effects come into the picture then heat flux at the bottom of the microchannel is no longer constant (Fig. 1a). This redistribution in heat flux alters the surface temperature, resulting in a varying wall to fluid temperature difference (ΔT); as against a constant ΔT for uniform heat flux boundary condition (Figs. 1c,d). It is noteworthy that heat flux can be further redistributed by employing geometry of varying cross section (Fig. 1b). The idea presented in this work makes use of these two effects (conjugate and varying cross section) in order to reduce the surface temperature gradient in a diverging microchannel.

In the inlet part of the diverging microchannel the heat flux is high which leads to a higher temperature in this region (Figs. 1c,d). As the fluid moves downstream, the heat flux decreases steadily and the rate of heating also goes down. This results in relatively lower temperature rise in the downstream section. The conjugate effects lead to an axial back conduction which tends to reduce the temperature gradients further. So, in effect, the temperature difference between the inlet and outlet is reduced to a great extent leading to a nearly isothermal boundary condition in a diverging microchannel. It is worthwhile to underscore that *the proposed process is particularly advantageous in the sense that it utilizes a constant heat flux boundary condition which is practically easier to maintain but results in a near isothermal surface condition*.

To prove this concept, heating in diverging microchannel is undertaken with DI water as the working fluid. The bottom of the substrate is subjected to a constant heat flux boundary condition. A comprehensive study of the ensuing temperature distribution at the substrate bottom of the diverging microchannel is carried out experimentally as well as numerically (Section 4). A detailed parametric study has also been performed at various geometrical, thermo-physical and input conditions in order to understand their effect on the bottom wall boundary condition (Section 5). A model is also proposed to obtain the value of the surface temperature as a function of various governing parameters (Section 6). Finally, the design is demonstrated for PCR application (Section 7).

3. METHODOLOGY EMPLOYED

A brief description of the experimental and numerical methodologies employed in the present work is presented in this section.

3.1 Experimental Investigation

Figure 2 presents a schematic of the experimental setup employed in the measurements [16-18]. The experimental setup consists of separate water and electrical circuits. The pump used for pushing DI water through the microchannel provided volumetric flow rate ranging from 0.1 to 6 ml/min. A pressure gauge equipped with data acquisition system recorded the pressure drop across the microchannel. A similar data logging arrangement was employed for recording

temperatures. The temperatures were measured by thermocouples placed at the inlet and outlet of the microchannel as well as on the bottom surface of the microheater.

The microchannels employed for the purpose of experimental investigation were fabricated on silicon wafer using MEMS techniques, involving photo lithography and wet etching; using in-house fabrication facilities. The detailed fabrication process is discussed elsewhere [17]. The values of different geometrical parameters of the microchannel along with the associated uncertainties are provided in Table 1.

3.2 Numerical Investigation

In order to obtain additional local information of the relevant parameters, three-dimensional numerical simulations were performed. For this purpose a microchannel having the same dimensions as that of the experimental test section was modeled numerically. A straight section having length of 5 mm was placed before the inlet to ensure that the flow is hydrodynamically fully developed before entering the microchannel. The silicon substrate thickness and length of the microchannel were taken as 286 μm and 20 mm respectively. The 1 μm thick microheater was also modeled. Figure 3 shows the microheater-substrate-microchannel assembly; the 5 mm straight reservoir towards the bigger width size is however not shown in the figure.

The numerical simulations were performed using commercial package Fluent. The variation of fluid viscosity (μ) and thermal conductivity (k) with temperature (T) have been considered in the simulations. These are modeled as per the equations given below [19]:

$$\mu = cT^d \quad \text{for } 300\ \text{K} \le \text{T} \le 363\ \text{K} \qquad (1)$$

where c = 1.1×10^{11} and d = -5.7. Note that the viscosity of water decreases by about 69% with increase in temperature, over the temperature range considered. The thermal conductivity however increases linearly with increase in temperature, and was modeled as

$$k = a + bT \quad \text{for } 300\ \text{K} \le \text{T} \le 373\ \text{K} \qquad (2)$$

where a = 0.0033, b = 0.0019. The increase in thermal conductivity is 11% over the temperature range considered.

Semi Implicit Method for Pressure Linked Equations (SIMPLE) algorithm was employed to solve the momentum and energy equations. Second order discretization scheme was employed for pressure equation; the momentum and energy equations were discretized using Quadratic Interpolation for Convection Kinetics (QUICK). A grid independence test was systematically carried out and accordingly 450,000 cells were selected for the simulations. The Nusselt numbers from the simulations were validated against the experimentally obtained value for a number of cases; the two agreed within 7%. Further validation of local temperature values is discussed through Figs. 5 and 6 presented later. The simulations are therefore deemed to be validated.

4. PROOF OF THE PROPOSED DESIGN

The combined results from experimental and numerical investigations will be presented and discussed in this section. First, the surface temperature distribution in an 8^o diverging microchannel was compared with a straight microchannel having a uniform width of 1133 μm, depth of 86 μm, same solid thickness and material. Note that the width of uniform cross section microchannel has been selected based on the concept of equivalent hydraulic diameter [16]. The simulation was carried out at a mass flow rate of 8.33×10^{-5} kg/s (5 ml/min) with a constant heat flux of 4.8 W/cm^2 supplied at the bottom wall. Figure 4 shows that the surface temperature difference between the inlet and outlet was significantly higher for straight microchannel (11 ^{o}C) as compared to a diverging microchannel (1 ^{o}C). In the case of diverging microchannel, the heat flux magnitude at the inlet is higher since the surface area at the inlet is smaller (Fig. 4b). This leads to an increase in the surface temperature near the inlet of diverging microchannel. The surface area of the microchannel keeps on increasing as we move downstream which leads to a decrease in the heat flux absorbed. Hence, the surface temperature near the outlet side is reduced to some extent. Also, the temperature gradients in the solid created by the flowing liquid lead to an axial back heat conduction which tries to reduce the temperature gradient. We therefore find that the temperature rise in a diverging microchannel is much less than a straight microchannel under identical conditions. This result is further verified through experiments.

In order to make experimental measurements, the surface temperature was measured using a thermocouple positioned at different axial locations; and the temperatures were recorded under

steady state condition. The process was repeated over the entire length of the microchannel. Figure 5 shows the axial temperature variation for four different flow rates between 4.17×10^{-5} – 9.17×10^{-5} kg/s. The reduction in surface temperature gradient is particularly evident at higher flow rates. Therefore, for the present microchannel configuration it is possible to reduce the surface temperature variation below 2º C over a large part of the microchannel by maintaining 9.17×10^{-5} kg/s of water flow through a diverging microchannel.

In addition to the axial variation, lateral variation of the temperature was also measured at both inlet and outlet locations. From Fig. 6, it can also be seen that the surface temperature variations along the lateral direction were not significant; and the temperature can be more or less assumed to be constant along the transverse direction. The reason for such uniformity of temperature in the transverse direction is the fairly high thermal conductivity of the silicon substrate (148 W/m-K). Figures 5 and 6 also present comparison of experimental and numerical results; the two are clearly in good agreement.

The above results point to the fact that the surface temperature gradients reduce significantly for diverging microchannels. It can therefore be concluded that by judiciously varying the thermophysical properties and input parameters, a nearly isothermal wall boundary condition can be obtained for a diverging microchannel. In the next section, a detailed parametric study analyzing the effect of different geometrical, flow and thermo-physical properties on the wall boundary condition is undertaken to establish the above finding over a larger parameter range.

5. EFFECT OF OTHER PARAMETERS

A number of parameters affect the magnitude of axial back conduction and alteration in the heat flux distribution in the microchannel. These parameters are: geometrical (angle, length, depth, solid-to-fluid thickness ratio), thermo-physical (thermal conductivity ratio of solid-fluid), and input conditions (mass flow rate, heat flux). A detailed parametric study was carried out, as discussed under the subsequent subsections.

5.1 Effect of angle

The three angles considered here are 1, 4 and 8^o. The inlet width was fixed as 200 μm and simulations were performed for a mass flow rate of 5×10^{-5} kg/s with bottom of the substrate maintained at a constant heat flux of 4.8 W/cm^2. The idea of redistribution in flux and its effect on obtaining isothermal conditions has been demonstrated successfully in Section 4 for 8^o diverging microchannel. As the angle was increased from 1^o onwards, there was relatively sharper increase in the area. So, the heat flux absorbed along the length of the microchannel as well as the Reynolds number gradients (thus Nusselt number) decrease steeply. Therefore, with increase in angle, the surface temperature gradients reduced to a great extent as evident from Fig. 7. For example, surface temperature gradients ($\Delta T_s/L$; where (ΔT_s is the difference in surface temperature and L is the microchannel length) for 1, 4 and 8^o microchannel were observed to be 0.6, 0.35 and 0.3 ^{o}C/mm respectively.

The results therefore suggest that an increase in the angle leads to a reduction in the surface temperature gradient, and is therefore preferable. However, there is an upper limit to the angle (16^o), beyond which flow reversal will come into the picture [16]; flow reversal would significantly alter the flow in the microchannel and the associated temperature and heat flux distributions.

5.2 Effect of depth

Effect of microchannel depth was also analyzed by simulating for three different microchannel depths – 86, 120 and 200 μm; while keeping the solid to fluid thickness ratio constant along with rest of the geometrical parameters. Again the flow rate was maintained at 5×10^{-5} kg/s and the wall heat flux as 4.8 W/cm^2. Increasing the depth and maintaining a constant solid to fluid thickness ratio leads to a decreased Reynolds number (Re), which reduces the convection strength. As a result, the average surface temperature increases with increase in the microchannel depth, as can be observed from Fig. 8. Also, the surface temperature gradient is observed to decrease with depth. It can be observed that the gradients are 0.3, 0.2 and 0.1 ^{o}C/mm respectively for 86, 120 and 200 μm microchannels. This is because the reduction in Re with depth is more towards the narrower region. Therefore, the convection effect drops largely towards the narrower end, which leads to an increase in the surface temperature. On the contrary, towards the larger

end the drop in Re is not much and hence an increase in the surface temperature at this end is small which brings in the constant wall temperature condition.

The microchannel depth therefore has an important effect on the temperature distribution; choosing a larger depth is advantageous from the point of view of maintaining a constant surface temperature.

5.3 Effect of length

In the next set of simulations, the effect of microchannel length on the ensuing surface temperature gradient was analyzed. The microchannel lengths considered were 10, 20 and 30 mm with all other geometrical parameters remaining the same. The mass flow rate was maintained at 5×10^{-5} kg/s and the bottom wall was supplied with a constant heat flux of 4.8 W/cm^2. Figure 9 shows a nearly isothermal surface condition (~1 °C) for 10 mm length microchannel. It was further observed that as the length reduced, the surface temperature gradient also reduced. For 10, 20 and 30 mm length microchannels, the temperature gradients were respectively 0.10, 0.30 and 0.53 ^{o}C/mm. The reason behind this nature is the decrease in the convection effect with length. The decrease in Reynolds number for 30 mm length microchannel is substantially higher than that of 10 mm length microchannel. As a result the 30 mm length microchannel shows a larger surface temperature gradient owing to reduced strength of convection in the downstream direction.

This result leads to a significant conclusion that a shorter length leads to a more uniform temperature distribution. Having a uniform temperature over a small length is particularly useful for microdevices.

5.4 Effect of solid to fluid thickness ratio

Conduction in solid becomes significant when the solid to fluid thickness ratio exceeds unity [12-15]. In order to examine the effect of solid to fluid thickness ratio on the surface temperature, the base case having $t_s/t_f = 2.32$ was compared against $t_s/t_f = 1.5$ and $t_s/t_f = 4$. Microchannel depth was maintained constant as 86 μm while the solid thickness was varied appropriately to obtain the desired ratio. This was done while maintaining all other geometrical parameters same as the

base case. Again, the heat flux was maintained at 4.8 W/cm^2 and the mass flow rate was kept 5×10^{-5} kg/s for this set of simulations.

It was observed that the surface temperature gradients reduce when t_s/t_f increases owing to an increase in the strength of axial back conduction due to the increase in solid cross sectional area (Fig. 10). However for the range of values considered here, the difference in surface temperature gradient is insignificant. A drastic variation of t_s/t_f is required to observe substantial change in the surface temperature distribution.

5.5 Effect of solid to fluid thermal conductivity ratio

Simulations were also performed to study the effect of solid conductivity (k_s) to fluid conductivity (k_f) ratio with working fluid fixed as water. For this purpose, the base case was taken as silicon (k_s/k_f = 247) and the results compared against steel (k_s/k_f = 27) and copper (k_s/k_f = 646) as the microchannel substrate materials. The heat flux was again maintained as 4.8 W/cm^2 and the mass flow rate as 5×10^{-5} kg/s. Since conductivity ratio is the only variable, it affects the intensity of axial back conduction. Increasing the conductivity ratio reduces the thermal resistance (L/k_sA; where L is the microchannel length and A is the cross section area) to axial back conduction. Therefore, the average surface temperature reduces for silicon and copper as compared to steel (Fig. 11). The temperature gradients come out to be 0.35, 0.3 and 0.28 ^{o}C/mm for steel, silicon and copper, respectively.

The above results suggest that unless the conductivity ratio is varied drastically, a substantial effect on the surface temperature gradients will not be seen. That is, the results presented in this study using silicon wafer is equally applicable to many other solid-liquid combinations as well. Any material which does not react with the biological sample and has a good thermal conductivity can be employed to make microchannels, making this methodology all the more attractive.

5.6 Effect of mass flow rate

Additional simulations were performed for 8^o diverging microchannels in order to observe the effect of mass flow rate on the temperature distribution at the bottom surface. The mass flow rates considered were 2, 3 and 5 ml/min at supplied heat flux of 4.8 W/cm^2 keeping all other

geometrical parameters same. It is observed that the surface temperature gradient as well as the average surface temperature reduced substantially at higher flow rates (Fig. 12). The temperature gradients for 2, 3 and 5 ml/min are 0.45, 0.3 and 0.05^{o}C/mm respectively. At higher flow rates, the convection heat transfer becomes substantially higher than the wall conduction. Therefore the relative magnitude of conjugate effect is reduced with an increase in the flow rate.

Hence, both lowering of the average surface temperature as well as the reduction of surface temperature is brought about at higher flow rates. However, employing higher flow rate would lead to a higher pressure drop penalty and should therefore be avoided. The constancy of the wall temperature should rather be maintained by suitably altering some other parameter.

5.7 Effect of heat flux

Simulations were also performed in order to study the effect of heat flux supplied at the bottom wall. The mass flow rate of 5×10^{-5} kg/s was passed through a 8° diverging microchannel at three different heat fluxes of 2.4, 4.8, 9.6 W/cm^2. The average temperatures went down with reduction in heat flux as expected (Fig. 13). Along with that, the temperature gradients were observed to be 0.1, 0.3 and 0.65 ^{o}C/mm for 2.4, 4.8 and 9.6 W/cm^2, respectively. Again a near constant surface temperature was observed for lower heat flux. That is, a higher heat flux leads to a higher temperature in addition to a higher temperature gradient.

Combining the results of this section with Section 5.3, it is noted that a lower heat flux over smaller segments of length is better than a higher heat flux over a larger length from the point of view of maintaining a nearly isothermal surface condition.

5.8 Summary of the parametric study

The experimental and numerical results showed that the combination of varying cross-section and conjugate effects lead to a redistribution of heat flux which significantly alters the wall heat flux boundary condition. This also affects the temperature distribution in the microchannel. A detailed parametric study was carried out to study the effect of different geometrical, thermo-physical and input parameters on the wall boundary condition which also provides an idea about the relative strength of convection and wall conduction in diverging microchannel.

Table 2 presents a summary of the parametric study. It is observed that the temperature gradient ($\Delta T_s/L$) decreases asymptotically with divergence angle (Case I). This could be attributed to a reduction in Reynolds number and heat flux at inner walls in the downstream direction with increase in angle. In Case II, it is observed that the average surface temperature increases with depth of microchannel owing to a decrease in Re. However, $\Delta T_s/L$ is observed to reduce with depth since the change in Re is more towards the narrower region as compared to the wider region. In Case III, the length of the microchannel was varied and it was found that a shorter length microchannels exhibits better surface temperature homogeneity (lower $\Delta T_s/L$). The reason for this is larger convection in shorter length microchannel (Re is higher) than in longer one with same angle of divergence. Also, there is a reduction in the resistance to the axial back conduction with decrease in length of microchannel. In the next two cases (Cases IV and V), the effect of conjugate heat transfer on $\Delta T_s/L$ was studied. In this, solid to fluid conductivity ratio and thickness ratio were varied and it was concluded that only a drastic variation in these parameters would have a significant bearing on the surface temperature variation. Furthermore, the effects of input parameters were studied. It was found that increasing the mass flow rate reduced the temperature gradient ($\Delta T_s/L$). After this, simulations were performed by varying the substrate bottom wall heat flux and greater temperature homogeneity was observed when the heat fluxes were lower in magnitude.

In view of the detailed parametric study, the design parameters to achieve a nearly isothermal condition can be selected within the limit prescribed for the important parameters as: divergence angle (8-16^o), depth (> 86 μm) and length (< 20 mm) of microchannel along with mass flow rate (>3 ml/min) and heat flux (< 4.8 W/cm^2). Hence, it can be concluded from the parametric study that under the set of optimal parameters, diverging microchannel would yield a near isothermal boundary condition (±0.5 ^{o}C).

6. MODEL FOR ESTIMATING THE SURFACE TEMPERATURE

This section presents a model for estimating the surface temperature as a function of the various governing parameters. The role of various governing parameters in the direction of achieving

isothermal wall condition has been identified in the previous section. Accordingly, a diverging microchannel with divergence angle: θ, depth: H and length: L is considered.

Consider a control volume of diverging microchannel as shown in Fig 1b. Using energy balance over the control volume we can write at steady state:

$$\dot{E}_{in} = \dot{E}_{out} \tag{3}$$

where, $\dot{E}_{in}$ and $\dot{E}_{out}$ are respectively the net energy entering and leaving the control volume. Now, based on the above parametric study, it is assumed that most of the energy gets convected with the flow. Therefore, we can write Eq. 3 as,

$$dq''(x)P(x)dx = \dot{m}c_p dT_f \ , \tag{4}$$

where, $q''(x)$ is heat flux supplied (W/m^2), $P(x)$ is the perimeter of diverging microchannel (m), $\dot{m}$ is the mass flow rate (kg/s), c_p is the specific heat capacity (J/kg-K), and T_f is local fluid temperature (K). Integration of Eq. 4 can be shown to give

$$T_f(x) = T_{f,i} + \frac{q}{\dot{m}c_p L}x \tag{5}$$

where $T_{f,i}$, and q are the inlet temperature (K) and power (W) supplied to the diverging microchannel of length L (m). Eq. 5 gives the variation of local fluid temperature $T_f(x)$.

Now consider a nearly isothermal wall boundary condition, Eq. 4 can be re-written as

$$\dot{m}c_p \frac{dT_f}{dx} = h(x)P(x)\Delta T \ , \tag{6}$$

where $h(x)$ is the convective heat transfer coefficient (W/m^2-K) and ΔT is the difference between surface and fluid temperatures, i.e. $\left(T_s - T_f\right)$ in K. For nearly isothermal wall boundary condition we assume that ΔT varies with the same rate as T_f, i.e., $-\frac{d\left(\Delta T\right)}{dx} \approx \frac{dT_f}{dx}$. (This assumption is evaluated towards the end of the section.) Therefore, Eq. 6 becomes;

$$\frac{d(\Delta T)}{\Delta T} = -\frac{h(x)P(x)}{\dot{m}c_p}dx \ , \tag{7}$$

Eq. 7 can be integrated from inlet to outlet assuming that *h* is a constant calculated at the characteristic location for diverging microchannel [16]:

$$\int_{\Delta T_i}^{\Delta T_o} \frac{d(\Delta T)}{\Delta T} = -\frac{h}{\dot{m}c_p}\int_0^L P(x)dx \tag{8}$$

The heat transfer coefficient can be obtained from a known correlation for Nusselt number:

$$h = \frac{Nuk_f}{D_h} = \frac{\alpha \,\mathrm{Re}^{\beta} k_f}{D_h} \tag{9}$$

where $\alpha = 0.301$ and $\beta = 0.563$ are obtained from the curve fitting of experimentally derived Nusselt number versus Re curve (not shown). In the above equation, k_f is the thermal conductivity of fluid (in W/m-K) and Reynolds number can be calculated from $\mathrm{Re} = \frac{\dot{m}D_h}{A\mu}$. The hydraulic diameter $D_h = \frac{4A}{P}$ where, A, P are the cross sectional area and perimeter of diverging microchannel calculated at the characteristic location. The characteristic location lies at L/3 from the inlet [16].

After some algebra, Eq. 8 yields

$$\left(T_{s,o} - T_{s,i}\right) = \left(T_{s,i} - T_{f,i}\right)\exp\left[-\frac{hL}{\dot{m}c_p}\left(w_i + L\tan\left(\frac{\theta}{2}\right) + 2H\right)\right] - \left(T_{s,i} - T_{f,i} - \frac{q}{\dot{m}c_p}\right) \tag{10}$$

from which the average surface temperature can be obtained as

$$\begin{aligned}\overline{T_s} = {} & \frac{1}{2}\left(\frac{qD_h}{\alpha \,\mathrm{Re}^{\beta} k_f PL}\right)\exp\left[-\frac{\alpha \,\mathrm{Re}^{\beta} k_f L}{D_h \dot{m}c_p}\left(w_i + L\tan\left(\frac{\theta}{2}\right) + 2H\right)\right] \\ & + \frac{1}{2}\left(2T_{f,i} + \frac{qD_h}{\alpha \,\mathrm{Re}^{\beta} k_f PL} + \frac{q}{\dot{m}c_p}\right)\end{aligned} \tag{11}$$

in terms of the relevant governing parameters.

The surface temperature from Eq. 11 has been validated against experimental data in Table 3. The model clearly predicts the experimental data in the various cases tested to within 1 ºC. The slightly higher value predicted by the model could be because we have neglected the effect of conduction heat flux in the model.

The above model, which has a strong theoretical basis, is therefore reasonably accurate. There are two main assumptions involved in the derivation of the model: (i) ΔT varies with the same rate as T_f, and (ii) h calculated at the characteristic location is representative over the entire microchannel. These assumptions are required to avoid unnecessary mathematical complexity without comprising the accuracy of the predictions. The effect of these assumptions is apparently small, at least for the parameter range considered here, as evident from the comparison in Table 3. We believe that these assumptions are not too severe even otherwise.

The model can be used to predict the temperature that the surface will attain for a given set of parameters. The model can further help in deciding the optimal design parameters of diverging microchannel in order to achieve a nearly isothermal boundary condition. The model was indeed utilized in this latter manner for PCR application as presented in the next section.

7. APPLICATIONS AND SIGNIFICANCE OF THE DESIGN

In certain biological applications where maintaining a constant temperature (typically 37^{o}C) is of utmost importance in order to keep the cells alive, there is a need to design portable systems which can maintain the desired temperature [1, 2]. Our results show that this is possible and the desired temperature can be maintained within ±0.5 ºC. In order to achieve the same objective, researchers [6,7,11] have proposed ingenious albeit intricate ways. The appeal of the proposed method lies in its simplicity. *By allowing a liquid to flow through a diverging microchannel supplied with constant heat flux at its bottom wall, a constant temperature can be achieved at the microchannel walls*. The proposed design therefore adds portability to the existing processes by eliminating the need of an incubator. This also suggests that for a given geometry and properties

of diverging microchannel, *any constant wall temperature* can be obtained by changing the input parameters appropriately (i.e. with the help of Eq. 11).

We now demonstrate our concept on a more complex example of PCR. The objective here is to maintain the different stations at the required temperatures of 95, 55, 72 °C (as explained in Section 1) so that PCR can be effectively carried out on a single chip. Three thermally insulated differently optimized diverging microchannels connected in series are employed for this purpose (Fig. 14a). The microchannels have different depths and different input heat fluxes. All the geometrical and input parameters are selected based on our model (Eq. 11). The results are obtained numerically and presented in Fig. 14b. The results are extremely encouraging in that three constant temperatures (~95, 57 and 73 ºC) can be achieved in the three diverging microchannels with heat flux of 10.5, 0.09 and 3.8 W/cm^2, for mass flow rate of 5×10^{-5} kg/s. The proposed design is therefore an important step forward in successful implementation of various lab-on-chip technologies.

8. CONCLUSIONS

In this study, we show that microchannel of varying cross section brings about redistribution in heat flux; also wall conduction (or conjugate effect) comes into picture at microscales. These effects can be exploited to our advantage to obtain a constant wall temperature surface condition. Heating in microchannels was studied numerically and experimentally in order to observe the effect of redistribution in heat flux and the ensuing surface temperature gradient. A comparative study performed between straight and 8^o diverging microchannels showed a significant reduction in the surface temperature gradient for the latter case, lending credence to our proposition.

The proposed idea was also verified experimentally in an 8^o diverging microchannel over a wide range of flow rates. The lateral distribution of temperature showed an insignificant variation while the axial temperature gradient reduces substantially; thus implying that the surface temperature is almost constant. A detailed parametric study of the effect of various geometrical (angle, depth, length and solid-to-fluid thickness ratio), thermo-physical (thermal conductivity of solid) and input parameters (mass flow rate and heat flux) on the microchannel surface was

undertaken to explore this finding over a wider parameter range. The outcome of this parametric study suggested the selection of important parameters as: divergence angle (8-16º), depth > 86 µm, length < 20 mm; along with mass flow rate > 3 ml/min and heat flux < 4.8 W/cm^2. For this set of optimal parameters, diverging microchannel would yield a nearly isothermal boundary condition with temperature difference between inlet and outlet of less than 1^{o}C.

A mathematical model is also proposed to obtain the optimal geometrical parameters for a given set of input parameters (mass flow rate and heat flux). Equation 11 derived in the paper can be employed for the purpose of designing the microchannel.

This constant temperature boundary condition in a diverging microchannel can be effectively utilized in certain biological applications where the samples are highly sensitive to temperature fluctuations. Finally, a successful demonstration of the proposed design is shown numerically for an on-chip PCR. The simple and novel approach presented here can be employed in several other applications as well.

9. REFERENCES

1. P.J. Hung, P.J. Lee, P. Sabounchi, R. Lin, L.P. Lee, Biotechnol. Bioeng., 2005, 89, 1–8.

2. Y. Wan, D. Tamuly, P.B. Allen, Y. Kim, R. Bachoo, A.D. Ellington, S.M. Iqbal, Biomed Microdevices, 2013, 15, 635–643

3. S. Makino, H. Cheun, Journal of Microbiological Methods, 2003, 53, pp. 141-147.

4. J.F. Regan, A.J. Makarewicz, B.J. Hindson, T.R. Metz, D. M. Gutierrez, T.H. Corzett, D.R. Hadley, R.C. Mahnke, B.D. Henderer, J.W. Breneman, T.H. Weisgraber, J.M. Dzenitis, Anal. Chem., 2008, 80, 7422-7429.

5. E.M. Janiszewska, L. Weglarz, M. Szczurko, BioMed Research International, 2013.

6. B. Selva, J. Marchalot, M.C. Jullien, J. Micromech. Microeng. 2009, 19, 065002 (1–10).

7. B. Selva, P. Mary, M.C. Jullien, Microfluid. Nanofluid. 2010, 8, 755–765.

8. T.M. Hsieh, C.H. Luo, F.C. Huang, J.H. Wang, L.J. Chien, G.B. Lee, Sens. Actuator. B 2008, 130, 848–856.

9. J.H. Wang, L.J. Chien. T.M. Hsieh, C.H. Luo, W.P. Chou, P.H. Chen, P.J. Chen, D.S. Lee, G.B. Lee, Sens. Actuator. B 2009, 141, 329–337.

10. A. Persat, J.G. Santiago, Twelfth International Conference on Miniaturized Systems for Chemistry and Life Sciences, October 12 - 16, 2008, San Diego, California, USA.

11. J. Wu, W. Cao, W. Chen, D.C. Chang, P. Sheng, Biofluidics 2009, 3, 012005:1–012005:7.

12. M. K. Moharana, G. Agarwal, S. Khandekar, Int. J. of Thermal Sciences, 2011, 50, 1001-1012.

13. G. P. Celata, M. Cumo, V. Marconi, S. J. McPhail, G. Zummo, Int. J. of Heat and Mass Transfer, 2006, 49, 3538-3546.

14. M. Rahimi, R. Mehryar, Int. J. of Thermal Sciences, 2012, 59, 87-94.

15. A.G. Fedorov, R. Viskanta, Int. J. of Heat and Mass Transfer, 2000, 43, 399-415.

16. V.S. Duryodhan, S.G. Singh, A. Agrawal, Microfluidics and Nanofluidics, 2013, 14, 53-67.

17. S.G. Singh, A. Kulkarni, S.P. Duttagupta, B.P. Puranik, A. Agrawal, Experimental Thermal and Fluid Science, 2008, 33, 153–160.

18. V.S. Duryodhan, S.G. Singh, A. Agrawal, Sadhana, 2013, 38, 1067-1082.

19. F.P. Incropera, D.P. Dewitt, T.L. Bergman, A.S. Lavine, Fundamentals of Heat and Mass Transfer, 6th ed. Wiley, 2007.

Table 1: Geometrical specification of the microchannel employed in the present study

Feature	**Size**	**Uncertainty**	**Units**
Smaller Width (W_i)	270	+ 2	μm
Larger Width (W_o)	3052	+ 2	μm
Length (L)	20	-0.1	mm
Height (H)	86	± 1	μm
Divergence Angle (θ)	8	0.5	°
Hydraulic Diameter (D_h)	157	1.33	μm

Table 2: Summary of Parametric study showing dependency of ΔT/L on each parameter.

(Case) Parameters	Wall Temperature gradient	Non dimensional Geometrical Parameters					Input Parameters		Remarks	
	$\Delta T_s/L$ (°C/mm)	θ	w/H	L/H	ts/H	ks/kf	m (ml/min)	q" (kW/m^2)		
(I) Effect of Angle	0.875	0	2	233	2.33	247	3	48	Strong function	Convection
	0.600	1	4	233	2.33	247	3	48		
	0.350	4	8	233	2.33	247	3	48		
	0.300	8	13	233	2.33	247	3	48		
(II) Effect of depth	0.300	8	13	233	2.33	247	3	48	Strong function	
	0.200	8	9	167	2.33	247	3	48		
	0.100	8	6	100	2.33	247	3	48		
(III) Effect of length	0.100	8	8	116	2.33	247	3	48	Strong function	
	0.300	8	13	233	2.33	247	3	48		
	0.533	8	19	349	2.33	247	3	48		
(IV) Effect of thickness	0.300	8	13	233	1.50	247	3	48	weak function	Conjugate
	0.300	8	13	233	2.33	247	3	48		
	0.300	8	13	233	4.00	247	3	48		
(V) Effect of Thermal conductivity	0.275	8	13	233	2.33	646	3	48	Moderate function	
	0.300	8	13	233	2.33	247	3	48		
	0.350	8	13	233	2.33	27	3	48		
(VI) Effect of Mass flow rate	0.450	8	13	233	2.33	247	2	48	Strong function	Convection
	0.300	8	13	233	2.33	247	3	48		
	0.050	8	13	233	2.33	247	5	48		
(VII) Effect of Heat flux	0.075	8	13	233	2.33	247	3	24	Strong function	
	0.300	8	13	233	2.33	247	3	48		
	0.650	8	13	233	2.33	247	3	96		

Table 3: Validation of proposed model with experimental data ($\overline{T_s}$ denotes average surface temperature).

Mass flow rate (kg/s)	Power Supplied (W)	$\overline{T_s}$,°C (Experimental)	$\overline{T_s}$, °C (Proposed model Eq. 11)	$\left(\overline{T_s}\big\|_{model} - \overline{T_s}\big\|_{expt}\right)$, °C
3.33×10^{-5}	3.5	49	50	1
5.00×10^{-5}	3.5	44	45	1
6.67×10^{-5}	3.5	41	42	1
8.33×10^{-5}	3.5	39	41	2
10.0×10^{-5}	4.0	40	41	1

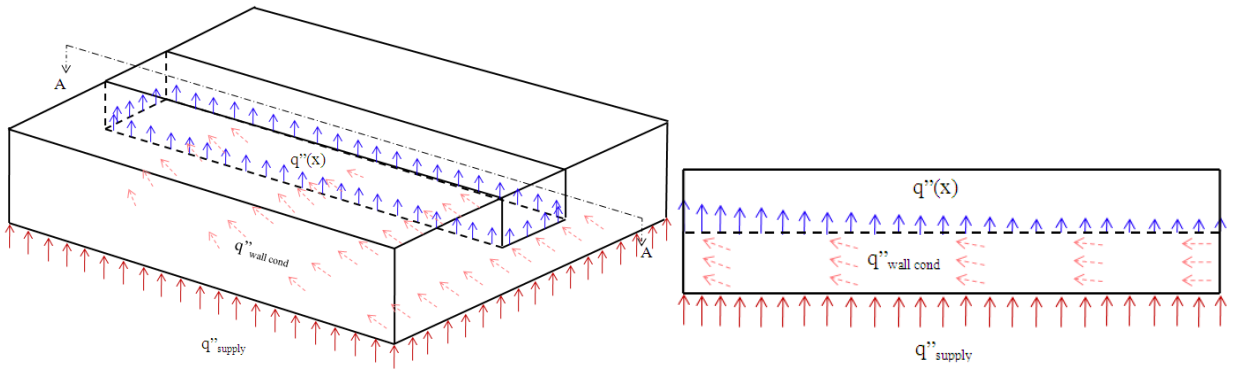
A
q''(x)
q''wall cond
q''supply
A
q''(x)
q''wall cond
q''supply

(a)

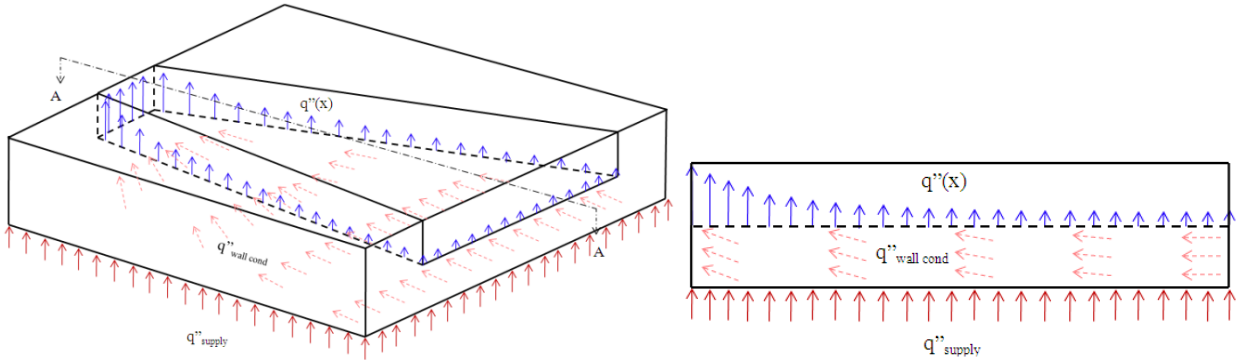
A
q''(x)
q''wall cond
q''supply
A
q''(x)
q''wall cond
q''supply

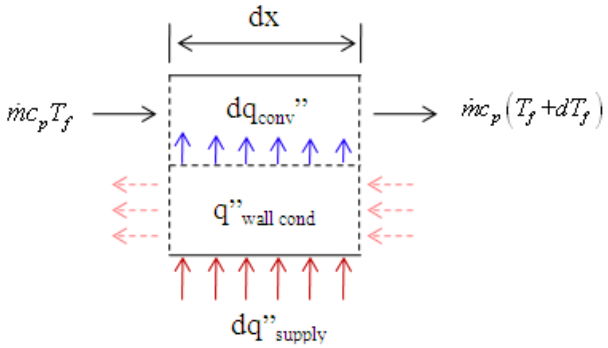
dx
$\dot{m}c_p T_f$
dq_{conv}''
$\dot{m}c_p\left(T_f + dT_f\right)$
q''wall cond
dq''supply

(b)

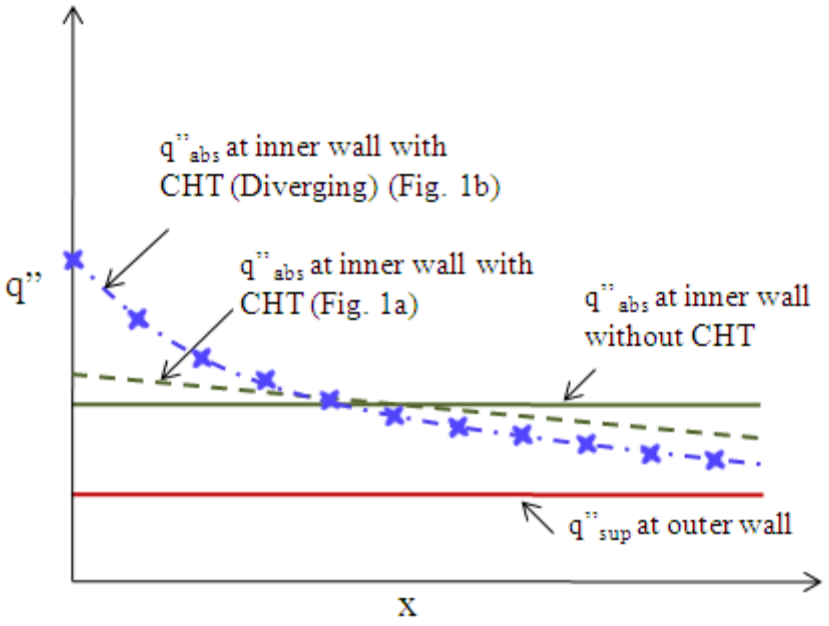

(c)

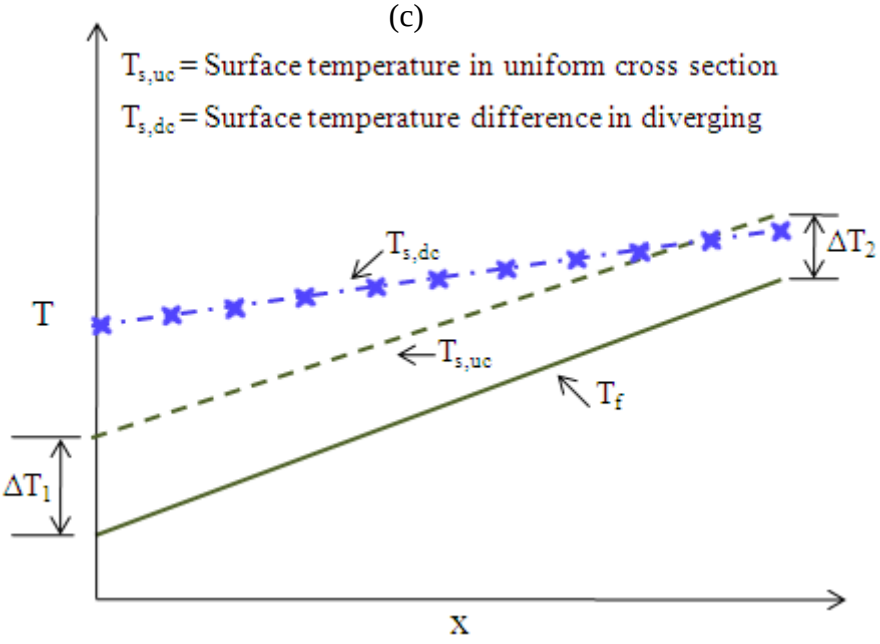

(d)

Figure 1: Schematic representation of the proposed method bringing about constant wall temperature condition. (a) and (b) show the heat flux at the walls for uniform cross section and diverging microchannel respectively. A graphical representation of the heat flux variation and temperature variation along the flow direction are provided in (c) and (d) respectively. (CHT stands for conjugate heat transfer.)

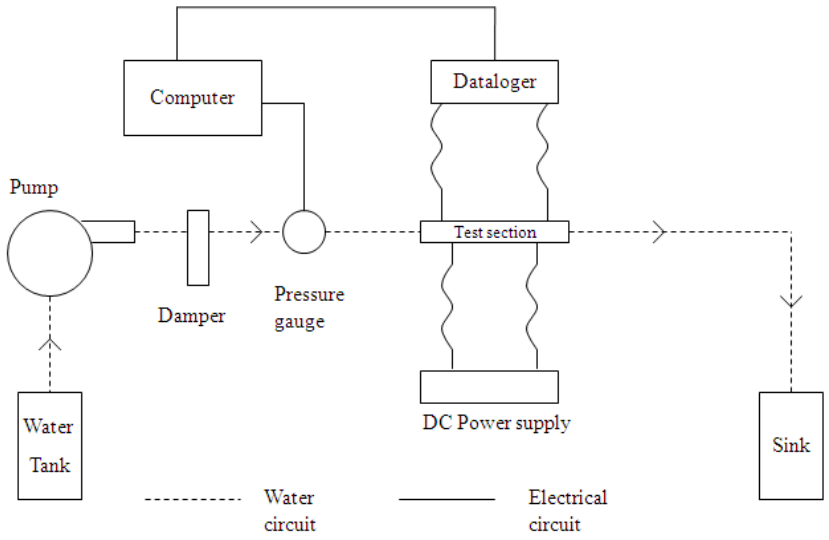

Figure 2: Schematic of the experimental setup

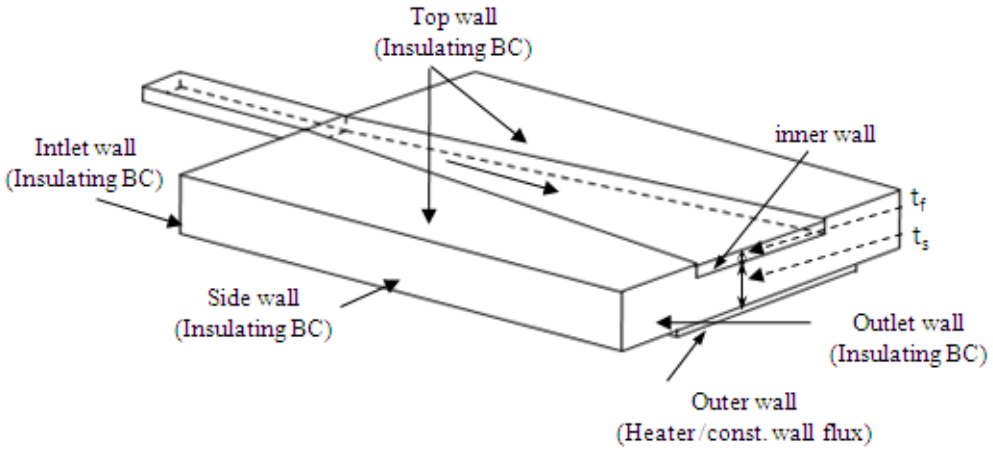

Figure 3: Three-dimensional model employed in the numerical simulations. A diverging (8º) microchannel with t_s/t_f = 2.32 (not to scale) is shown here.

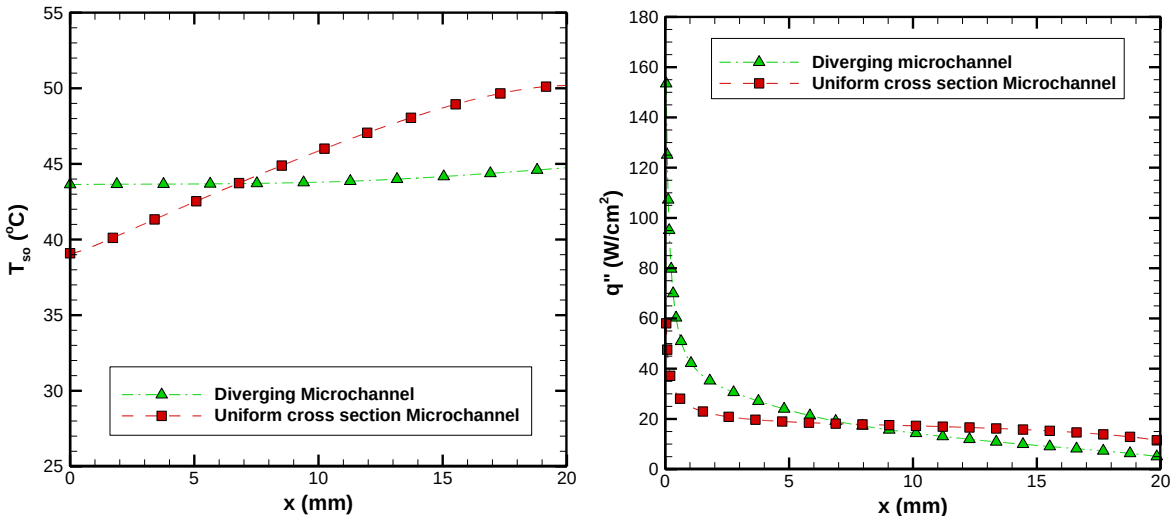

(a) (b)

Figure 4: Comparison of (a) surface temperature and (b) heat flux distribution in a diverging and a straight microchannel.

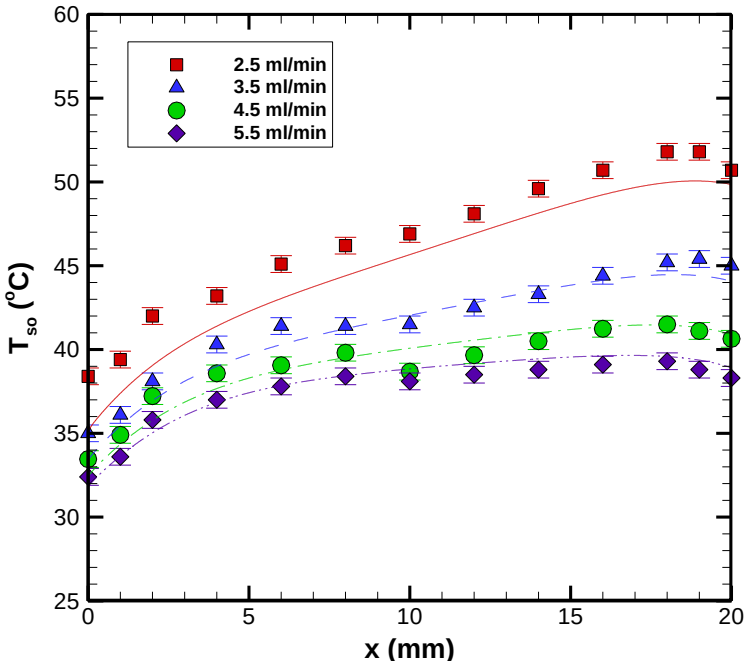

Figure 5: Surface temprature variation along the flow direction in a diverging microchannel at q'' = 4 W. (Symbols represent experimental data whereas lines show the corresponding numerical result.)

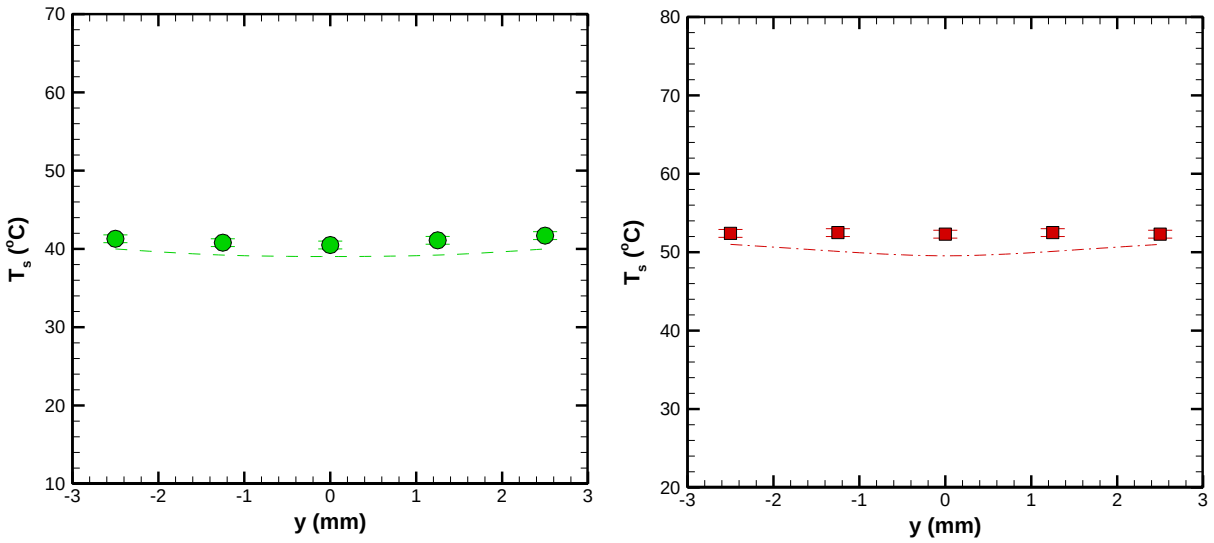

(a) Inlet (b) Outlet

Figure 6: Comparison of lateral surface temperature variation at (a) inlet and (b) outlet in a diverging microchannel, for m = 4.17×10^{-5} kg/s and q_{sup} = 4 W. (Symbols represent experimental data whereas lines show the corresponding numerical result.)

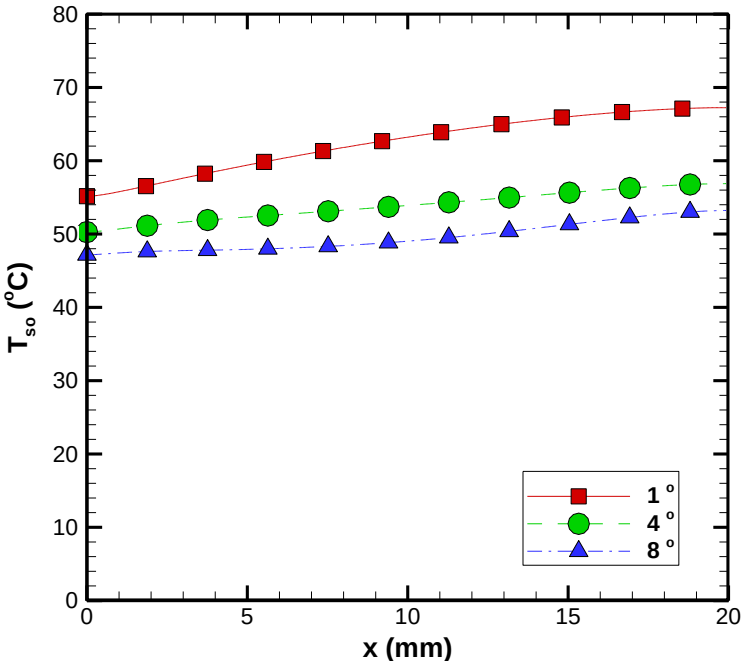

Figure 7: Effect of angle on surface temperature variation in diverging microchannel.

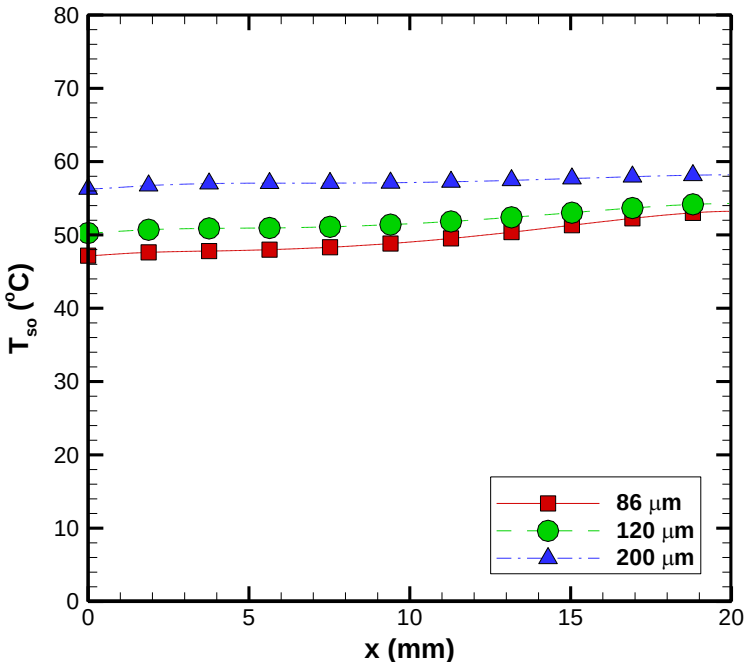

Figure 8: Effect of depth variation on surface temperature distribution in diverging microchannel

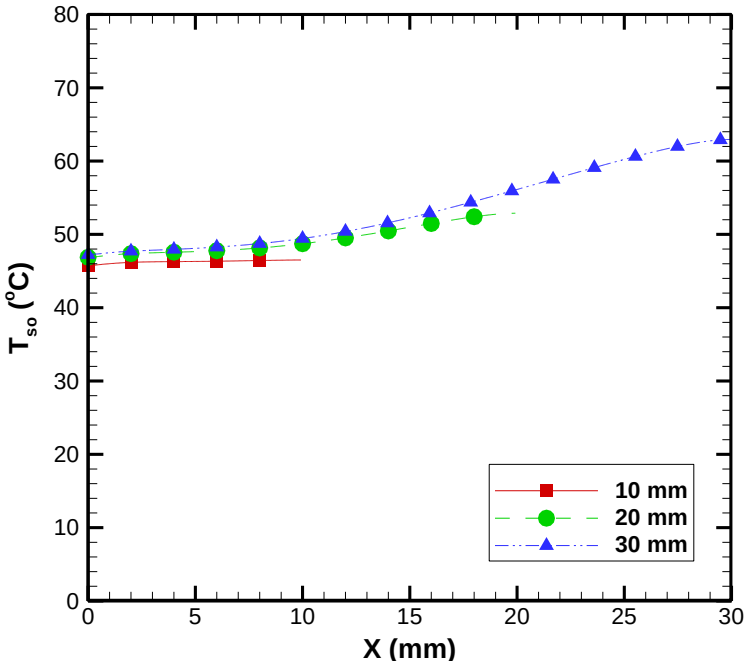

Figure 9: Effect of length on surface temperature distribution in diverging microchannel.

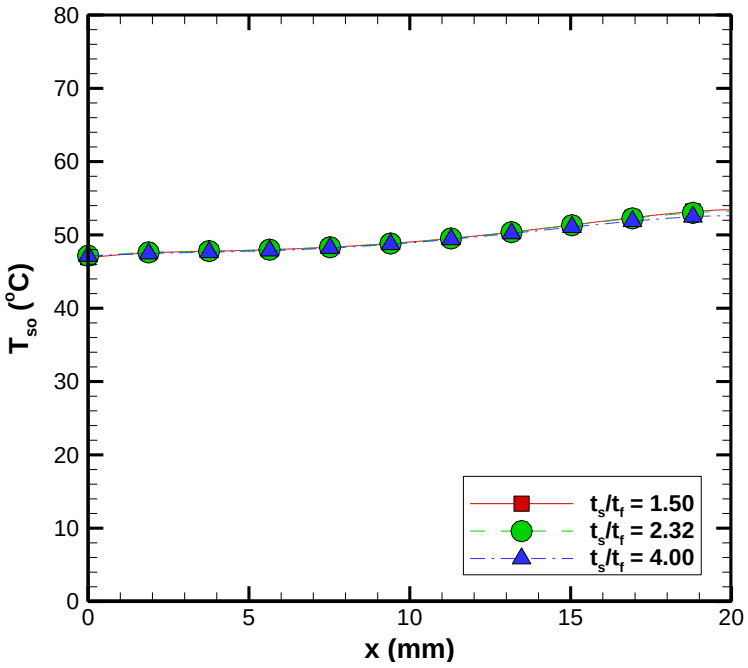

Figure 10: Effect of t_s/t_f variation on surface temperature distribution in diverging microchannel.

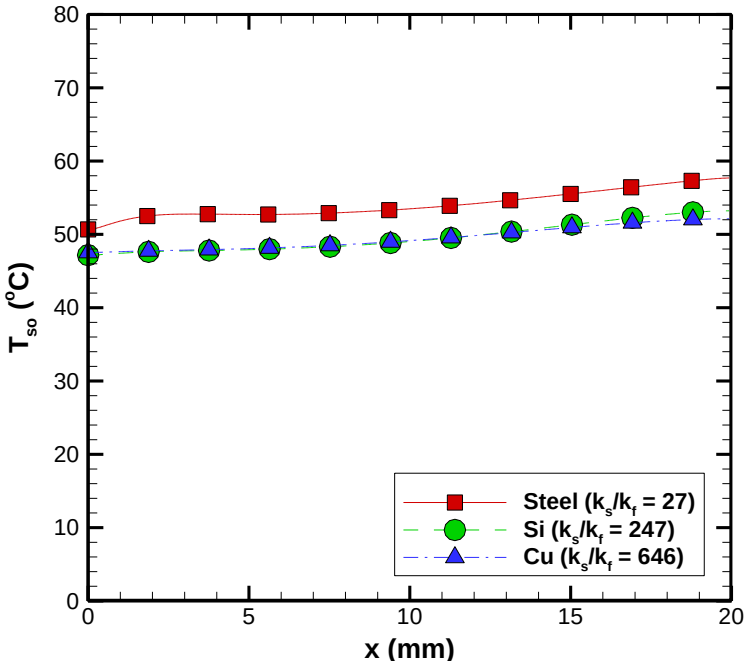

Figure 11: Effect of solid to fluid conductivity ratio on surface temperature variation in diverging microchannel.

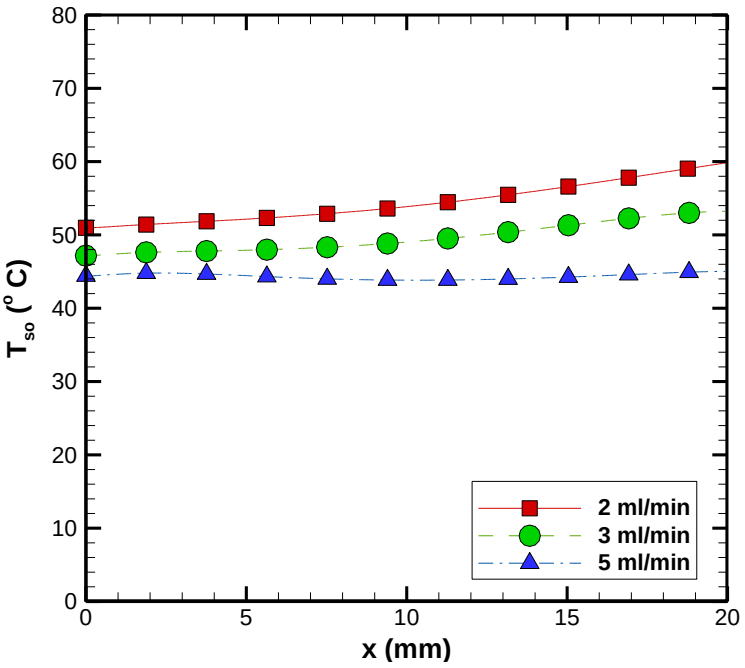

Figure 12: Effect of mass flow rate on surface temperature distribution in diverging microchannel.

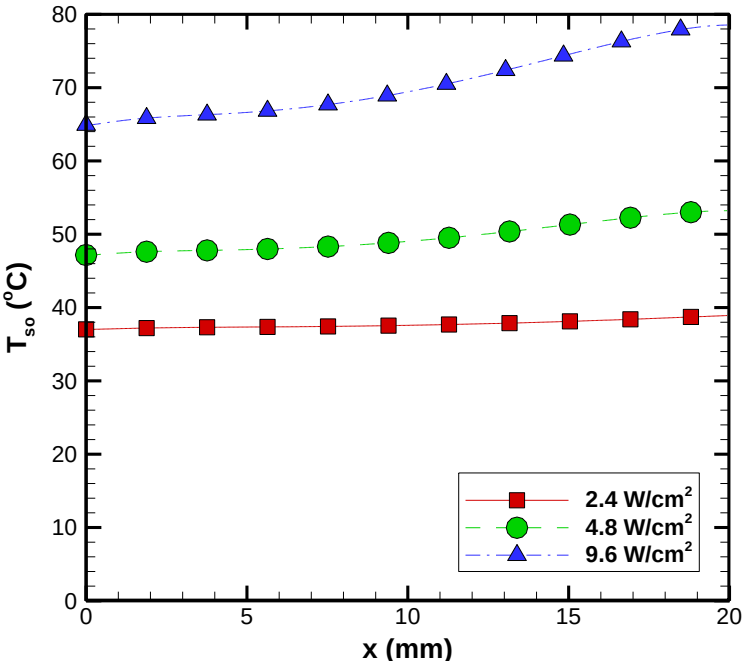

Figure 13: Effect of heat flux variation on surface temperature distribution in diverging microchannel.

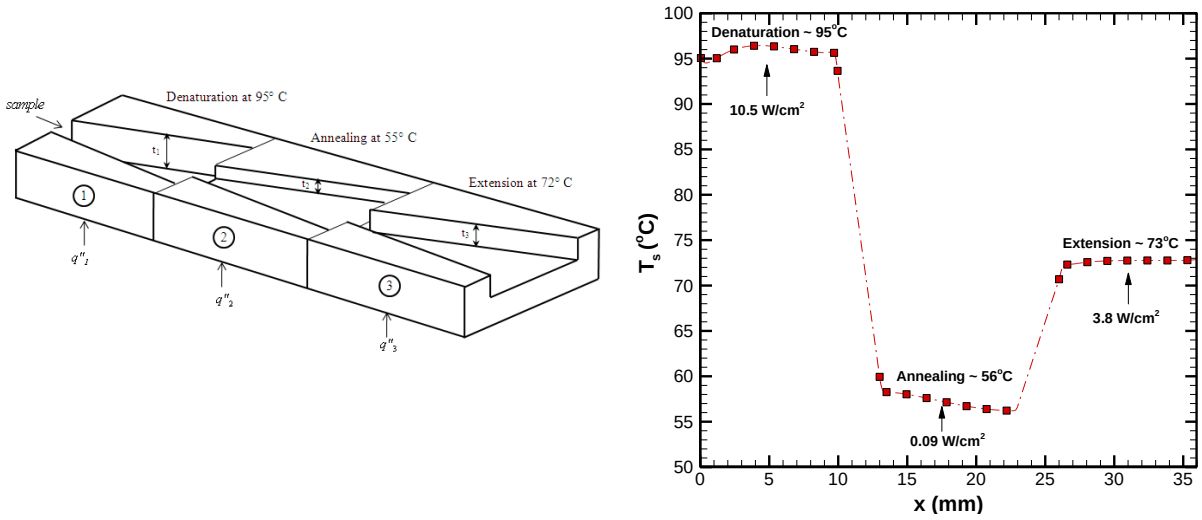

(a) (b)

Figure 14: (a) Schematic representation of a microdevice for on-chip PCR process. The microdevice consists of three diverging microchannels of different geometrical configurations. (b) The temperature profile in the three stations (diverging microchannels).